Test Method for Contactless On-wafer MEMS Characterization and Production Monitoring

Sarah Linz, *Student Member, IEEE*, Florian Oesterle, Stefan Lindner, *Student Member, IEEE*, Sebastian Mann, *Student Member, IEEE*,
Robert Weigel, *Fellow, IEEE*, and Alexander Koelpin, *Member, IEEE*

***Abstract*—Micro-electro-mechanical systems (MEMS) are widely utilized in various devices ranging from consumer electronics and medical devices to modern industrial equipment. Their fabrication with the help of semiconductor technology leads to very low-cost devices. However, the fabrication test systems need to be extended to cover the mechanical domain of MEMS devices. Therefore, this paper presents a new concept that is able to evaluate the stiffness of silicon membranes in MEMS microphones. Due to the use of electromagnetic waves in the millimeter wave spectrum an optical line-of-sight is not necessary. The test set-up can be parallelized to improve the throughput and it can gain important feedback information to tune operating parameters of the production process.**

***Index Terms*—MEMS characterization, contactless testing, mechanical sensitivity, millimeter wave metrology, pull-in**

I. Introduction

MICRO-Electro-Mechanical Systems (MEMS) are nowadays employed as innovative, miniaturized sensors for a huge variety of applications ranging from industrial sensors [1], [2] to consumer electronics [3], [4] and medical devices [5]. Shrinking electro-mechanical components down to micrometer scale with the help of sophisticated semiconductor technology involves three main advantages: integration of MEMS components into systems with electronic integrated circuits and improved sensor characteristics while reducing the costs due to high-volume production [3].

Consumer electronics like mp3-players or video cameras and communication devices like mobile phones employ MEMS microphones because of their compact size, little weight and high audio signal quality. To further improve sound quality by means of noise cancellation techniques, several microphones are integrated in one device leading to an even higher demand of MEMS microphones. Although classical electret condenser microphones are still available at a lower price than MEMS microphones, the latter ones obtain more and more market shares due to their reliability and sound quality.

For the optimization of the industrial fabrication process and reduction of manufacturing costs, well-established test methods of classical semiconductor production, for instance dedicated test structures to control process parameters and their local variation over the wafer, are employed. However, additionally, an evaluation of the mechanical characteristics of MEMS devices is necessary. Therefore, a test method for the mechanical characteristics will be presented in this work. It is based on a contactless millimeter wave measurement set-up that evaluates the movement of the microphone's membrane by detecting the reflected electromagnetic wave. An experimental verification of the measurement concept in upper millimeter wave spectrum including results is presented in this paper for the first time. The phase information of the wave needs to be extracted and therefore the system incorporates a new dedicated calibration procedure in the complex I/Q plane.

In the following section, the currently known or available methods for the characterization of MEMS microphones during the production process will be analyzed. In Sec. III the theory on MEMS microphones and interference in millimeter wave measurements will be presented, followed by the description and the evaluation of the new test method (Sec. IV) as well as the dedicated calibration procedure (Sec. V).

II. State of the Art

To detect out-of-specification sensors at the end of the manufacturing process, a final test of packaged sensors has to be conducted. Parallel testing is preferred because test time is crucial: the longer the test the more expensive the manufacturing process. Parallelized test set-ups are commercially available for different sensor types, for instance the *InPhone* MEMS strip test module from *multitest* for MEMS microphones.

Nevertheless, also fast on-wafer test methods are required to sort out defective dies prior to further production steps and packaging in order to avoid spending resources for faulty sensors. Moreover, an early detection of malfunctions can be used to readjust process parameters. A measurement directly after the wafer dicing may be preferable since the dicing changes the mechanical stress and therefore the sound sensitivity. The aim of the test is to measure the transfer function of the device, i.e., the ratio between the actuating force and the static or dynamic deflection. This is an indication for the mechanical stiffness and therefore for the sensitivity of the microphone.

To evaluate the deflection of a microphone's membrane, two methods are known: Contact-based measurement of electrical changes due to geometrical variations and contactless optical techniques.

Manuscript received —; —.

The authors are with the Institute for Electronics Engineering, Friedrich-Alexander University of Erlangen-Nuremberg, 91058 Erlangen, Germany, e-mail: {sarah.linz, florian.oesterle, stefan.lindner, sebastian.mann, robert.weigel, alexander.koelpin} @fau.de

This work was conducted within the project T-MEMS, which is funded as part of the program Mikrosystemtechnik by the Bavarian Ministry of State of Economic Affairs, Infrastructure, Traffic and Technology.

TABLE I
PARAMETERS OF MEMS MICROPHONE

parameter	R	T	d_0	w_0	A
value	448 µm	330 nm	2.2 µm	1.8 µm	0.63 mm^2

Contact-based methods apply a voltage between the electrodes leading to a movement of the sound-sensitive membrane towards or away from the counter electrodes depending on the polarity of the voltage. The resulting impedance variation is measured by an impedance analyzer using special probes for contacting the MEMS. This mechanical contact may induce stress and therefore distort the mechanical behavior of the MEMS as well as the measurement. Furthermore, for proper contacting, the device under test (DUT) has to be precisely positioned and shifted in z-axis, which is time-consuming.

Thus, contactless techniques are preferred. In literature, two approaches can be found: optical and radar based methods. The optical ones are often used for laboratory measurements, e.g., in [6], to verify the functionality and evaluate the response of the membrane to acoustic waves. Spatial resolution can be achieved with Michaelson or Twyman-Green interferometers by a lateral scanning of the DUT or by using a camera chip with the required spatial resolution [7], [8]. An overview can be found in [9]. For the detection of the dynamical characteristics optical interferometers have to be modified to include the strobe technique [10] or laser Doppler vibrometers [11], [12] have to be employed. Sophisticated commercial systems are available on the market, for example the *MSA-500 Micro System Analyzer* from *Polytec GmbH*. However, for the on-wafer test during the manufacturing process there is only one technique known to the authors that is able to measure the deflection of several MEMS DUTs in parallel: this technique uses 5x5 parallel micro optical interferometers measuring up to 25 DUTs at the same time [13], [14].

The disadvantage of optical methods is that they rely on an optical line-of-sight. This can often not be guaranteed during inline tests in semiconductor mass production [15], [16]. To overcome this drawback, a contactless test method has been proposed in [15] for the first time that uses electromagnetic waves in the millimeter wave spectrum. A proof of concept at 90 GHz with a commercial broadband Vector Network Analyzer (VNA) showed the applicability of the method [15] and further research investigated the influence of the chosen frequency band and a non-perforated chuck material that supports the DUT [16]. The VNA has been replaced in [17] by a dedicated receiver comprising a six-port interferometer with a test signal at 100 GHz. It has been shown, that this heterodyne concept with a six-port interferometer exhibits excellent phase resolution and is therefore suitable for the evaluation of the MEMS microphone's mechanical sensitivity.

In this work, the millimeter wave approach will be investigated in more detail. The parasitic couplings within the measurement set-up as well as reflections at the chuck material will be analyzed and a novel calibration technique will be presented, which is able to overcome this problem. These new findings are applicable for both, six-port and VNA measurements, and an arbitrary frequency range within the microwave and millimeter wave spectrum.

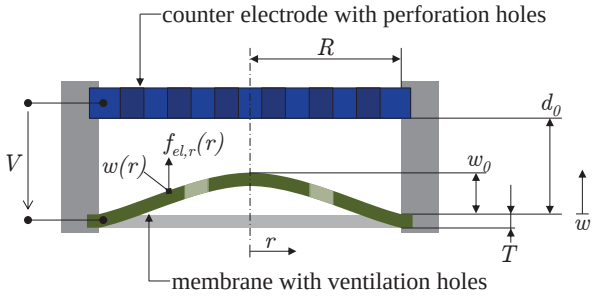

Fig. 1. Schematical view of the MEMS microphone under test (after [18]).

III. THEORY

A. Micromechanical analysis of MEMS microphone

A simplified schematical cross-section of the MEMS microphone is depicted in Fig. 1 and the relevant parameters are summarized in TABLE I. This configuration forms a capacitor with two circular electrodes, one of them, called membrane or diaphragm, being able to deflect towards or away from the other electrode. Acoustic waves can penetrate the highly perforated counter electrode through vias, also called acoustic holes, and deflect the sound sensitive circular silicon membrane. The membrane has the thickness $T = 330\,\text{nm}$. The capacitor is characterized by its radius $R = 448\,\mu\text{m}$ (area $A = 0.63\,\text{mm}^2$) and the distance $d_0 = 2.2\,\mu\text{m}$ between the electrodes in the non-excited state. The flexible membrane moves according to the varying pressure of the acoustic wave and causes a corresponding change in the capacitive coupling between membrane and counter electrode. This change can be detected and evaluated with an application specific integrated circuit (ASIC). The instantaneous deflection is described by the function $w(r)$ with the maximum swing w_0 in the center of the membrane.

The deflection can be induced also by applying a voltage V_{dc} between the electrodes. The characteristic change of the capacitance ΔC over this actuation voltage V_{dc} is illustrated in Fig. 2. For $V_{\text{dc}} = 13.75\,\text{V}$ a jump of the capacitance can be noticed. This unstable state is called pull-in phenomenon [19]. It is reached when the electrostatic force caused by the voltage V_{dc} is higher than the mechanical elastic restoring force of the membrane [20]. The force equilibrium cannot be obtained any more and thus the movable part of the microphone snaps towards the counter electrode. The corresponding pull-in voltage $V_{\text{dc}} = V_{\text{pi}}$ can be calculated from geometrical parameters of the microphone [19]:

$$V_{\text{pi}} = \sqrt{\frac{8kd_0^3}{27\epsilon_0 A}}, \tag{1}$$

where k is the spring constant, ϵ_0 the permittivity of vacuum and $A = \pi R^2$ the area of the electrodes. Since the pull-in voltage is very stable and simple to evaluate, some MEMS devices even use it as transduction mechanism [20], [22].

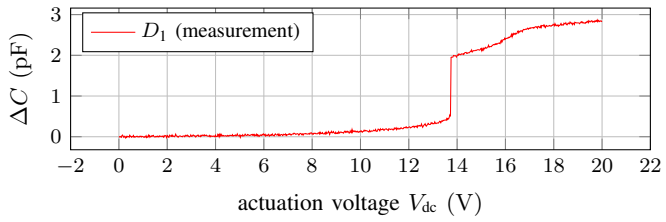

Fig. 2. Measured variation of capacitance over the actuation voltage between the MEMS's electrodes (data from [21]).

A large deflection model has been derived in [18] that allows to calculate the intrinsic stress of a membrane from the measured pull-in voltage under static conditions. Electrostatic force and mechanical restoring force are considered and calculated separately. The mechanical restoring force is related to the intrinsic stress σ_0, whereas the electrostatic force is connected to the voltage V_{dc}. Furthermore, it is demonstrated by measurement results that the considered MEMS microphone's deflection is very close to a pure membrane behavior. Therefore, the deflection at each position of the diaphragm can be approximated by [23]:

$$w\left(r\right) = w_0 \left(1 - \frac{r^2}{R^2}\right). \tag{2}$$

The decision whether membrane or plate behavior is dominant can be made by evaluating the tension parameter ξ [23]:

$$\xi = \sqrt{\frac{\sigma_0 R^2 T}{D}}, \tag{3}$$

depending on geometrical dimensions (T, R), residual stress σ_0 and stiffness D. ξ tends to zero for plate behavior and to infinity for membrane behavior.

Due to the almost ideal membrane behavior in the present case the mechanical restoring force is given by [18]:

$$F_{\mathrm{m}} = \frac{\pi 2 \xi^2 D}{R^2 \left(\frac{I_0(0) - I_0(\xi)}{\xi I_1(\xi)} + \frac{1}{2}\right)} w_0 = k_1 w_0, \tag{4}$$

with I_0 and I_1 being the modified Bessel functions of first kind (order zero and one) [24] and k_1 being the linear spring constant. The stiffness D can be calculated from the Young's modulus E, the membrane thickness T and the Poisson's ratio ν:

$$D = E \frac{T^3}{12\left(1 - \nu^2\right)}. \tag{5}$$

Furthermore, the electrostatic force is related to the voltage V_{dc} by [18]:

$$F_{el} = \frac{1}{2}\,\epsilon_0\,\pi\,R^2\,V_{\mathrm{dc}}^2 \left[\frac{\alpha_a d_0^2 + \alpha_b d_0 + \alpha_c}{d_0(d_0 - w_0)} - \alpha_a\right]. \tag{6}$$

The dense perforation of the counter electrode (Fig. 1) leads to a fringing electric field that varies with the deflection $w(r)$ and is described by the factors $\alpha_a, \alpha_b, \alpha_c$.

With (6), (4) and (3) the residual stress σ_0 can be calculated for the measured voltage $V_{\mathrm{dc}} = V_{\mathrm{pi}}$ at pull-in. However, for this it is necessary to detect the pull-in phenomenon. It can be done by measuring the capacitance between the electrodes (Fig. 2) with an impedance analyzer or by observing the membrane's movement.

Before introducing the system concept for the observation of this displacement with the help of millimeter wave electromagnetic signals, some theoretical aspects of reflections and parasitic interferences have to be discussed to better understand the concept and the calibration in the I/Q plane.

B. Ideal RF Reflection

The electrostatic actuation of the mechanical subcomponent induces a displacement. In the considered case this is the movement of the MEMS microphone's diaphragm. In microwave reflectometers this can be interpreted as a one-port measurement with varying distance between the VNA's reference plane and the DUT (Fig. 4). As known from network analysis [25], the scattering (S-) parameter $\underline{S_{11}}$ is the complex ratio of reflected ($\underline{b_1}$) and transmitted ($\underline{a_1}$) wave:

$$\underline{S_{11}} = \frac{\underline{b_1}}{\underline{a_1}} = \frac{b_1 e^{\mathrm{j}\phi_{\mathrm{b}}}}{a_1 e^{\mathrm{j}\phi_{\mathrm{a}}}} = S_{11} e^{\mathrm{j}\phi}. \tag{7}$$

In a theoretical, ideal case, the relative displacement Δw of the reflecting plane in the DUT would only change the argument of the reflected signal: $\phi_{\mathrm{b}} = \phi'_{\mathrm{b}} + \Delta\phi(\Delta w)$. Related to the unchanged reference signal, the deflection of the membrane can be directly given with the help of the argument of $\underline{S_{11}}$:

$$\phi = \phi'_{\mathrm{b}} + \Delta\phi(\Delta w) - \phi_{\mathrm{a}}. \tag{8}$$

Therefore, it is sufficient to evaluate the relative phase variation in order to detect the pull-in phenomenon. For actuation voltages $V_{\mathrm{dc}} > V_{\mathrm{pi}}$ the electromechanical stability cannot be reached anymore and the resulting jump of the deflection causes an abrupt change in the phase. The expected quantitative phase variation for an ideal displacement Δw of the reflecting plane can be calculated in relation to the wavelength λ of the test signal with frequency f_{meas}:

$$\Delta\phi(\Delta w) = 2 \cdot \Delta w \frac{360^\circ}{\lambda} = 2 \cdot \Delta w \frac{360^\circ f_{\mathrm{meas}}}{c} \tag{9}$$

The round trip path length $2 \cdot \Delta w$ must be used to account for the doubled distance covered by the electromagnetic signal due to the reflection.

The advantage of the relative phase measurement is specially useful for the analysis of real signals with additional parasitic reflections, but also for applications in industrial, non-ideal environments. For instance, different wafer chuck materials and thicknesses or other dielectric materials influence the absolute phase of the reflected signal. However, the characteristic step-like relative phase variation can be detected anyway, as long as the dynamic range of the measurement system is sufficient [16].

C. Interference Induced by Parasitics

A challenging task is to minimize all non-idealities of the system and to deal with them with the help of sophisticated calibration routines. Due to the very small geometrical dimensions of the membrane (TABLE I) and the deflection, already

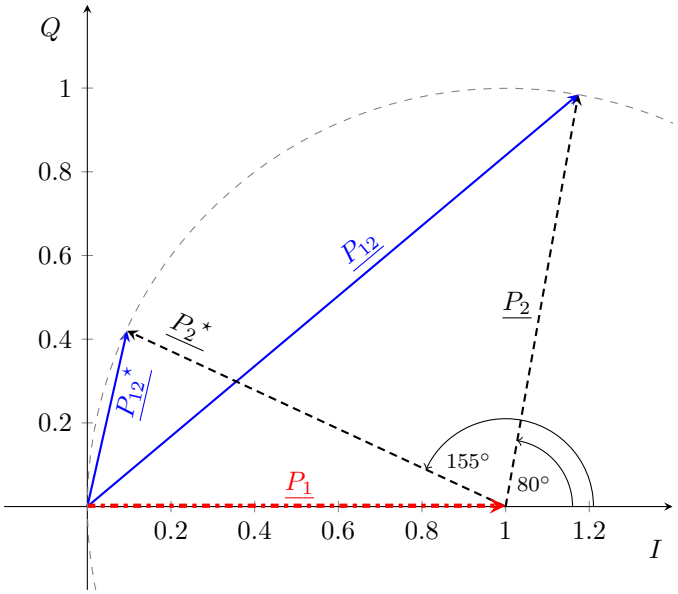

Fig. 3. Interference of the signal $\underline{S_1}$ with $\underline{S_2}$ and $\underline{S_2^\star}$, respectively.

the slightest non-ideality can have a dominant influence on the measurement results. All discontinuities and mismatches in the test set-up (Fig. 4) generate additional reflections:

- transition from air-filled waveguide to material with different permittivity
- impedance variation between chuck material and air-filled space underneath the membrane
- reflection of electromagnetic wave at the silicon substrate of the DUT
- reflection at the counter electrode in the case that the membrane is penetrated
- other reflection in the measurement set-up, such as contacting probe, cables, or microscope

All these reflections with different phase shifts sum up to a resulting parasitic signal with invariant frequency but different phasing. Fig. 3 illustrates the superposition of a signal $\underline{P_1}$ with the signals $\underline{P_2}$ and $\underline{P_2^\star}$, respectively. Depending on the phase between the superimposed signals, the resulting power level is lower (destructive interference) or higher (constructive interference) than the summed power levels of the original signals. As illustrated by Fig. 3, the 155° shift between $\underline{P_1}$ and $\underline{P_2}^\star$ results in destructive interference and therefore in a lower power level of the sum signal $\underline{P_{12}}^\star$. For phase shifts between -90° and +90°, constructive interference leads to a higher resulting power level. This is displayed by $\underline{P_{12}}$, the sum of $\underline{P_1}$ and $\underline{P_2}$ with a phase shift of 80°.

Compared to the phase shift caused by the deflection of the DUT, the parasitic reflections can be assumed as time-invariant. This static deviation of the overall reflected power leads to several relevant aspects for the analysis of the complex scattering parameter $\underline{S_{11}}$. The expected signal variation due to the deflection is influenced by the actual superposition of all reflections:

- The quantitative changes $\Delta\phi$ and ΔS_{11} can vary due to a change of the discontinuities (with unmodified movement of the membrane). Without calibration or suitable compensation, a measurement of the absolute displacement is not possible.
- In addition to the variation of the magnitude ΔS_{11}, also a positive or negative change of the phase $\Delta\phi$ can be expected when changing the position of the reflection plane.
- The absolute phase of each partial reflection is a function of frequency. This leads to a frequency dependent state of the static total superposition. Thus, the change of ΔS_{11} and $\Delta\phi$ due to the parasitic signal is also a function of frequency.

IV. System Concept

To detect the step-like deflection at pull-in, different frequency ranges between 90 GHz and 295 GHz have been evaluated with conventional network analysis techniques as well as with the six-port interferometric principle. Measurement results in W band with a commercial VNA have been reported in [15], [16] and with a dedicated six-port receiver in [17]. The focus of the following sections will be put on new measurements in upper millimeter wave spectrum (220 - 325 GHz) and the novel calibration approach for the system.

The lower frequency band [15]–[17] has been evaluated for measurements, because COTS- (commercial off the shelf) components are available in this band at the moment. However, an evaluation at higher frequencies is interesting, since the measured phase variation $\Delta\phi$ is proportional to f_{meas}. Considering (9), it is clear, that for a given membrane's deflection Δw, which is very small, a higher frequency (shorter wavelength) leads to an increasing measurable phase variation $\Delta\phi$. Furthermore, higher frequency waveguide components have a smaller cross section. For example, a W band waveguide ($75 - 110$ GHz, WR 10) has a cross section of 3.23 mm^2, whereas the area of a WR 3 waveguide ($220 - 325$ GHz) is 0.37 mm^2 and thus smaller than the area of the MEMS membrane. The larger the waveguide cross section is in comparison to the MEMS membrane, the more power is reflected by the surrounding equipment and not by the DUT, which causes parasitic interferences as explained in section III-C. However, there is one major drawback of the frequency range at 290 GHz: the measurement equipment is, at the moment, still very expensive and only few components are available. Although the technology is pushing forward, up to now there are only applications for space and research at these frequencies, mostly using passive sensors. Nevertheless, due to the mentioned advantages investigations at 290 GHz are very interesting for future application.

A. Measurement Set-up

Fig. 4(a) depicts a schematical view of the system concept. The bottom side of the microphone (DUT) is open for acoustic reasons. Therefore, electromagnetic waves can propagate from the open WR 3 waveguide to the microphone's membrane. At the interface between the media air and poly-silicon the wave is partly reflected back to the waveguide. The waver chuck is specially designed and optimized for this application as

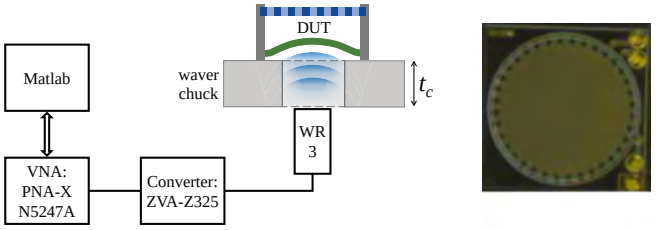

(a) Test set-up (b) DUT, top view

Fig. 4. Schematical view of the system concept.

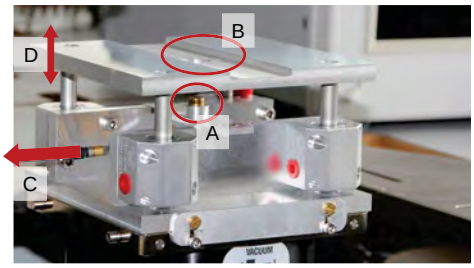

Fig. 5. Photo of the measurement adapter: (A) open waveguide, (B) placeholder for PTFE waver chuck, (C) to ZVA-Z325 converter, (D) height adjustable support for wafer

described in [16] and adapted for the corresponding frequency band. The PTFE wafer chuck has a thickness $t_c = 0.5\,\text{mm}$ and a perforation hole with radius $r_c = 0.45\,\text{mm}$, which is approximately the same dimension as the membrane's radius R. Fig. 5 shows a photo of the measurement adapter supporting the DUT (Fig. 4(b)), whereas a photo of the complete measurement set-up is depicted in Fig. 6.

When applying a continuous wave (CW) test signal with stable phase, the transversal deflection of the membrane causes a shift of the reflection plane and thus a shift of the reflected signal's phase. For the measurements between 220 GHz and 325 GHz, the VNA PNA-X N5247A (*Agilent Technologies*) generates the test signal and detects the reflection. To extend the available frequency range to 325 GHz, the millimeter-wave converter ZVA-Z325 (*Rohde & Schwarz GmbH Co. KG*) is used. The actuation voltage V_{dc} applied to the MEMS microphone with an electrical contact is swept from 0 to 20 V. Matlab is used for controlling the measurement and analyzing the collected data.

When testing on wafer level with numerous microphones, the voltage can be applied to all devices at the same time. Thus, a direct contact of one microphone is not necessary. For the proof of concept, diced MEMS microphones have been used (Fig. 4(b)).

B. Uncalibrated Measurement Results

The proper functioning of this new, innovative test method is proved in the following by measurement results. Each plotted data point is derived by calculating the arithmetic mean of five measured values.

Fig. 7 shows the relative change of the measured, uncompensated S-parameters at $f_{\text{meas}} = 290.2\,\text{GHz}$. The measured S-parameters present the characteristic jump at the pull-in

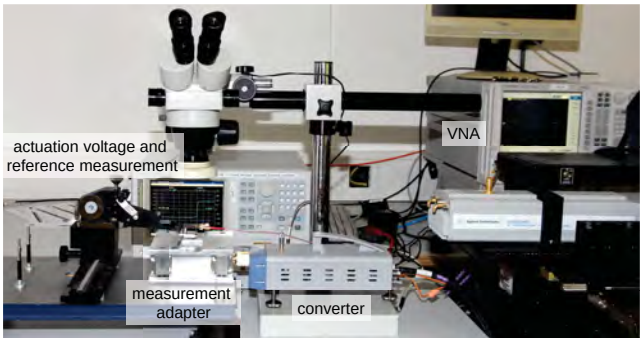

Fig. 6. Photo of the measurement set-up.

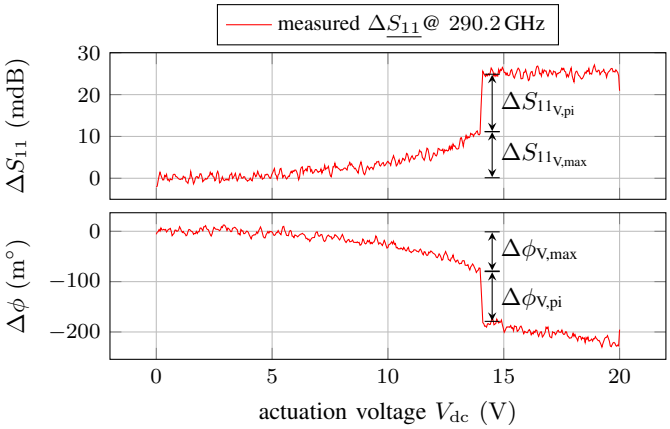

Fig. 7. Relative change of phase and magnitude of reflected test signal without calibration (displacement of membrane in the sub-micrometer range).

voltage of 13.75 V in both, the amplitude and phase. Even for voltages below 13.75 V a static change of $\Delta\underline{S_{11}}$ indicates the deflection of the membrane in the sub-micrometer range.

Besides the proof of the measurement concept, the results also demonstrate the impact of static reflections (Sec. III-C). Although the set-up is not changing, the magnitude of $\Delta\underline{S_{11}}$, i.e., the power level of the reflected signal, increases with the membrane's deflection. Furthermore, the phase of $\Delta\underline{S_{11}}$ decreases only by $\Delta\phi = 0.22°$. Assuming a maximum deflection of $w_0 = 1.8\,\mu\text{m}$, the ideal phase variation at $f_{\text{meas}} = 290.2\,\text{GHz}$ would be $\Delta\phi = 1.25°$ according to (9). A new compensation strategy for these effects will be derived in Sec. V.

Fig. 8 depicts the scattering parameter $\underline{S_{11}}$ of the complete measurement set-up over the frequency range from 289 GHz to 292 GHz. Both, magnitude (a) and phase (b), show a frequency-dependent characteristic for the case that the MEMS microphone is not actuated. Thus, also a frequency-dependent variation of $\underline{S_{11}}$ can be expected for a varying actuation V_{dc}. In Fig. 8 (c) and (d) the change of $\underline{S_{11}}$ for the maximum actuation voltage (V_{max}, blue circles) and at pull-in (V_{pi}, red stars) over the frequency range demonstrates the varying sensitivity of the given set-up. The maximum sensitivity for the magnitude can be achieved at 290.44 GHz and for the phase the extreme values can be found at 290.3 GHz and 290.6 GHz. Thus, the choice of a suitable operation point is essential.

According to these results it would be a possible solution

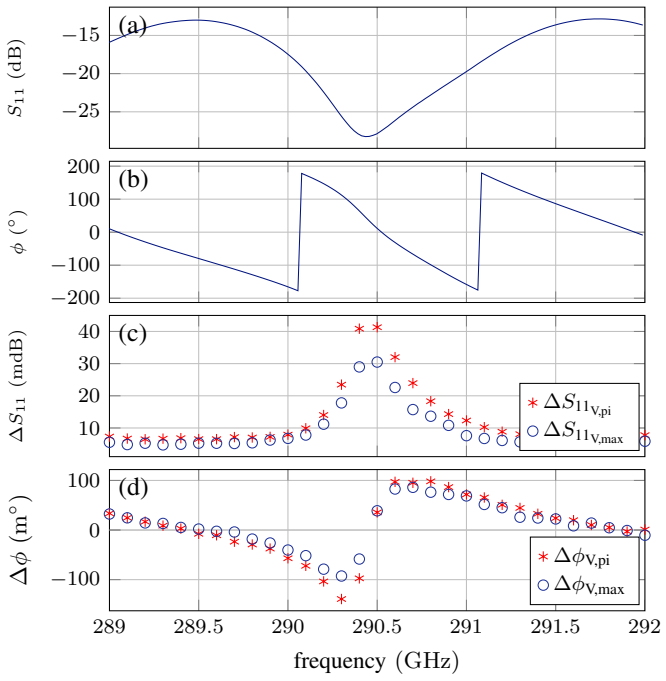

Fig. 8. Measured $\underline{S_{11}}$ of the complete set-up: (a) magnitude, (b) phase for a constant DC voltage $V_{\mathrm{dc}} = 0\,\mathrm{V}$; extracted change of (c) magnitude and (d) phase for an increasing DC voltage V_{dc} prior to the pull-in.

to limit the measurement to either a magnitude or a phase evaluation and to choose a suitable frequency with high sensitivity. In this case, no further calibration would be needed. However, this would implicate the loss of 50% of the available information and, what is even more crucial, that the variation of the operating point would strongly influence the measurement results. All, even small changes in the measurement set-up like thermal expansion, noise, or a frequency drift of the test signal could severely change the results due to a shift of the operating point. Therefore, in the following section a calibration procedure will be discussed which allows the use of both, magnitude and phase of $\underline{S_{11}}$, and thus of 100% of the acquired information.

The placement of a new DUT can also shift the operating point. However, the major static reflections arise from the measurement setup excluding the DUT. The additional offset in the I/Q plane caused by the individual DUT and its membrane is small and not relevant for the relative displacement measurement of the presented approach.

For an investigation of the measurement uncertainty the data at 291.5 GHz will be analyzed in the I/Q plane (Fig. 9). The standard deviation has been calculated from 140 measurement points for the in-phase and the quadrature signal:

$$\sigma_I = 1.51{\cdot}10^{-5}\,\mathrm{mW/W}; \qquad \sigma_Q = 1.45{\cdot}10^{-5}\,\mathrm{mW/W} \quad (10)$$

Furthermore, the size of the step at pull-in can be calculated by subtracting the data point at $V_{\mathrm{dc}} = 14.0\,\mathrm{V}$ from the data point at $V_{\mathrm{dc}} = 14.08\,\mathrm{V}$:

$$\Delta I_{pi} = |I_{14.08\,\mathrm{V}} - I_{14\,\mathrm{V}}| = 7.32 \cdot 10^{-5}\,\mathrm{mW/W}, \quad (11)$$

$$\Delta Q_{pi} = |Q_{14.08\,\mathrm{V}} - Q_{14\,\mathrm{V}}| = 1.71 \cdot 10^{-4}\,\mathrm{mW/W}. \quad (12)$$

This demonstrates that the signal to be measured (step size ΔI_{pi}, ΔQ_{pi}) is significantly higher than the measurement uncertainty due to noise.

V. MEMS Specific Compensation Approach

In order to evaluate the deflection of the microphone's membrane a calibration method will be derived in this section that compensates all static reflections in the measurement set-up. In contrast to conventional VNA measurements this calibration does not require special calibration standards.

Due to the linear superposition of the reflections, they can be canceled with the help of the resulting total vector. However, it's a challenge to find this vector when dedicated calibration standards are not available. Waveguide calibration standards could be used at the end of the waveguide antenna, but such a calibration would only include reflections up to the antenna. All other imperfections of the measurement set-up (Sec. III-C), e.g., reflections at the chuck material supporting the MEMS device, cannot be eliminated with this approach. For the evaluation of the membrane's displacement, calibration standards on wafer level would be necessary: either dedicated test chips with calibration structures or a sufficient variation of the membrane's position. Since the manufacturing of dedicated test chips is very time and cost intensive, the second solution will be investigated in this work.

For an absolute and complete calibration of the measurement set-up, a shifting of the reflection plane by approximately 360° is needed. In this set-up 360° corresponds to half a wavelength due to the double path length (round trip) of the reflected signal. For a smaller shifting, an ellipse fitting method can be applied to obtain calibration parameters [26], [27]. However, in the upper millimeter wave spectrum and with the silicon microphones as DUT even the maximum displacement of the membrane is not sufficient for the fitting. Therefore, an analytical solution for the calculation of the compensated, relative phase information will be derived, that eliminates the frequency dependency discussed before. This is possible due to the known step height of the device's membrane. For the derivation, the measured $\underline{S_{11}}$ is plotted in linear scale in the complex plane (Fig. 10) where I represents the in-phase component (real part) and Q the quadrature component (imaginary part) of $\underline{S_{11}}$:

$$I = S_{11}\cos\phi; \qquad Q = S_{11}\sin\phi. \quad (13)$$

As an example for the calibration procedure, Fig. 9 shows the measured $\underline{S_{11}}$ in the I/Q diagram at $f_{\mathrm{meas}} = 291.5\,\mathrm{GHz}$. $A(A_{\mathrm{I}}, A_{\mathrm{Q}})$ represents the deflection for $V_{\mathrm{dc}} = 0\,\mathrm{V}$ (minimum actuation) and has been calculated using the first 25 measured values, whereas $B(B_{\mathrm{I}}, B_{\mathrm{Q}})$ has been calculated from the last 25 values where $V_{\mathrm{dc}} = 20\,\mathrm{V}$ (maximum actuation, $V_{\mathrm{dc}} > V_{\mathrm{pi}}$).

For low actuation voltages the measured values are located very close to each other due to the small mechanical deflection. An increasing actuation voltage leads to a stronger deflection. In ideal or ideally calibrated measurement systems, this results in a pure phase shift, which is noticed as a circle around the origin of the I/Q plane. Because of the parasitic reflections in the real set-up, the increasing actuation voltage can be noticed

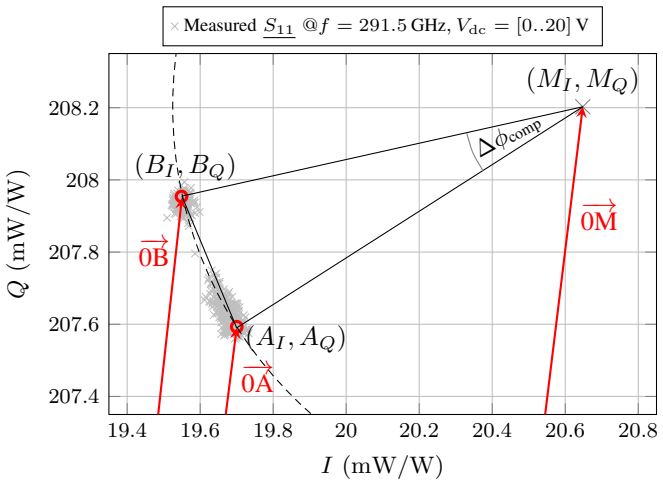

Fig. 9. I/Q diagram of the uncalibrated measurement data: extracted mean value for minimum (A) and maximum (B) actuation voltage, calculated static reflections (M).

in the I/Q diagram as a reduced value of the measured in-phase component and a simultaneously increasing value of the quadrature component. This corresponds to an arc of a circle not centered around the origin.

Although the sampling rate is constant and the actuation voltage is increased linearly during the measurement, the measured values are not distributed homogeneously because of the non-linear transfer function. For the pull-in phenomenon there is only one measurement value between A and B that marks the almost instantaneous jump of the membrane (instantaneous in relation to the sampling rate).

The reflections measured with the test set-up are composed of a linear superposition of the reflection at the dynamic target (i.e., the moving membrane) and all static reflections within the set-up. Assuming a constant reflected power $S_{11_{\mathrm{comp}}}$ at the moving target and a measurement system with linear characteristic, all measured values are located on a circle with the center representing the sum of all static reflections $\overrightarrow{0\mathrm{M}}$. The position of the measured values (including points A and B, Fig. 9) on the circle is related to the membrane's deflection and is described with the phase angle $\Delta\phi_{\mathrm{comp}}$.

From Fig. 9 it is clear that the reconstruction of the circle only with the help of the measurement data is very unstable and imprecise since the covered distance of the membrane is very small compared to the wavelength in the considered frequency range. Therefore, the angle $\Delta\phi_{\mathrm{comp}}$ is calculated using (9) and the assumption from Sec. III-A (TABLE I) that the mechanical displacement between the points A and B is $w_0 = 1.8\,\mu\mathrm{m}$:

$$\begin{aligned}\Delta\phi_{\mathrm{comp}}\,(w_0 = 1.8\,\mu\mathrm{m}) &= 1.8\,\mu\mathrm{m} \cdot 2\tfrac{360^\circ f_{\mathrm{meas}}}{c} \\ &= 1.25^\circ.\end{aligned} \tag{14}$$

With this additional information, a geometrical reconstruction of the circle center M and with this of the complete circle is possible. The geometric reconstruction is illustrated in Fig. 9 (not to scale) with a triangle between A, B and M, and the analytically determined angle $\Delta\phi_{\mathrm{comp}}$.

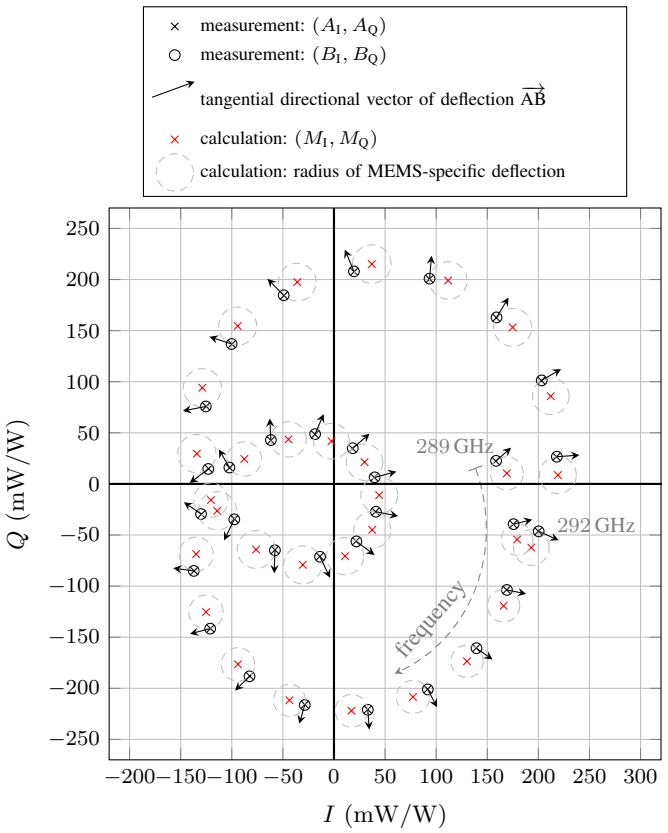

Fig. 10. Measured I/Q values over the whole frequency range, calculated static reflections (x) and tangential vector that represents the phase variation due to the membrane's movement.

Mathematically, the reconstruction of the circle center $M = M(M_I, M_Q)$ as the terminal point of the vector $\overrightarrow{0\mathrm{M}}$, can be described with the following equations:

$$\begin{aligned} M_{\mathrm{I}} &= \tfrac{1}{2}[A_{\mathrm{I}} + B_{\mathrm{I}} + \tfrac{1}{\cot(\frac{\Delta\phi_{\mathrm{comp}}}{2})}(-A_{\mathrm{Q}} + B_{\mathrm{Q}})], \\ M_{\mathrm{Q}} &= \tfrac{1}{2}[A_{\mathrm{Q}} + B_{\mathrm{Q}} + \tfrac{1}{\cot(\frac{\Delta\phi_{\mathrm{comp}}}{2})}(-A_{\mathrm{I}} + B_{\mathrm{I}})]. \end{aligned} \tag{15}$$

Knowing the vector $\overrightarrow{0\mathrm{M}}$ of the static reflections in the test set-up, the offset can be compensated, i.e., calibrated measurement data can be obtained.

For the considered frequency range between 289 GHz and 292 GHz with a stepsize of 100 MHz all circle centers have been reconstructed with the proposed calibration method and are shown in Fig. 10. Due to the rescaling, the initial and terminal points (A, B) can optically not be separated any more. For this reason, small vectors indicating the membrane's direction of movement ($\overrightarrow{\mathrm{AB}}$) have been introduced. This illustration also points out the challenge of the measurement set-up: the phase variation, that has to be determined, is very small and hard to separate from the strong static reflections.

After a calibration of the test set-up (Fig. 4), compensated measurement data is obtained. The compensated $\underline{S_{11}}$ is plotted in Fig. 11 in the I/Q plane. The mean power of the calibrated data is shown as a red circle centered around the origin of the I/Q plane. Thus, the power level is now almost independent of the frequency.

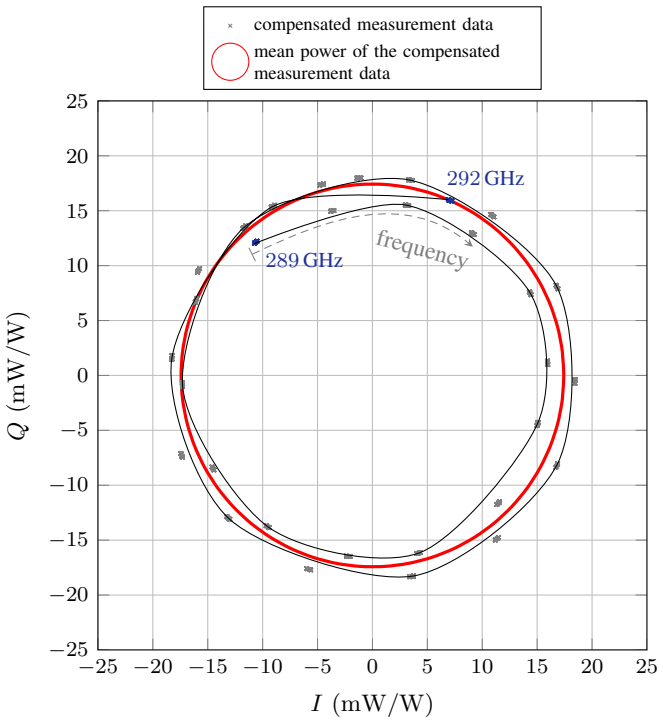

Fig. 11. Compensated $\underline{S_{11}}$ between 289 GHz and 292 GHz in the I/Q plane.

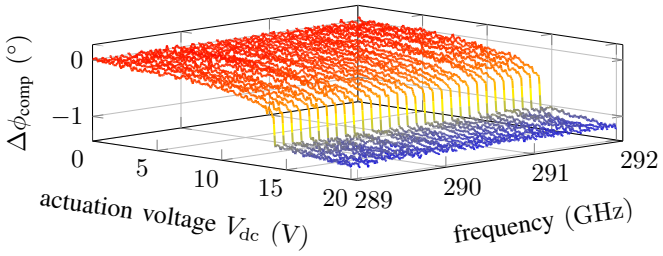

Fig. 12. Measured phase variation for the considered frequency range after calibration.

As a last step, the phase variation due to the moving membrane during actuation ($V_{\text{dc}} = [0, ..., 20]$ V) is calculated from the compensated measurement data and depicted in Fig. 12. Although the measurement set-up shows a strongly varying reflection coefficient over the frequency range, the phase variation is constant over the frequency if the proposed calibration procedure is applied.

VI. Conclusion

This paper presented a comprehensive analysis of a new measurement concept for the industrial test of MEMS microphones by millimeter wave metrology. The detailed investigation of parasitic reflections within the test set-up led to a new calibration procedure, that has also been developed within this work. For the first time, the measurements of the MEMS' silicon membrane's movement have been conducted in the frequency range between 289 and 292 GHz. This frequency range has two main advantages: it enables the application in optical non-line-of-sight scenarios and it is also excellent for very precise displacement measurements due to the very short wavelength.

Measurements showed that the new concept is very promising for the implementation in the semiconductor production process of MEMS microphones. The concept can help to reduce test time, detect defective devices before packaging and therefore, it can contribute to a more efficient, low-cost manufacturing of MEMS microphones. Furthermore, the measurements can deliver important information about the manufacturing process that can be used to tune operating parameters for a further improvement of the MEMS' performance.

Acknowledgment

The authors wish to thank F. Fink and H. Kuhn from the Department THA and A. Dehe (Infineon Technologies AG) for their helpful support.

References

[1] W. Hortschitz, H. Steiner, M. Sachse, M. Stifter, F. Kohl, J. Schalko, A. Jachimowicz, F. Keplinger, and T. Sauter, "Robust precision position detection with an optical mems hybrid device," *IEEE Trans. Ind. Electron.*, vol. 59, no. 12, pp. 4855–4862, Dec 2012.

[2] R. Dean and A. Luque, "Applications of microelectromechanical systems in industrial processes and services," *IEEE Trans. Ind. Electron.*, vol. 56, no. 4, pp. 913–925, April 2009.

[3] B.-H. Kim and H.-S. Lee, "Acoustical-thermal noise in a capacitive mems microphone," *IEEE Sensors J.*, vol. 15, no. 12, pp. 6853–6860, Dec 2015.

[4] I. Shahosseini, E. Lefeuvre, J. Moulin, E. Martincic, M. Woytasik, and G. Lemarquand, "Optimization and microfabrication of high performance silicon-based mems microspeaker," *IEEE Sensors J.*, vol. 13, no. 1, pp. 273–284, Jan 2013.

[5] C.-L. Wei, Y.-C. Lin, T.-A. Chen, R.-Y. Lin, and T.-H. Liu, "Respiration detection chip with integrated temperature-insensitive mems sensors and cmos signal processing circuits," *IEEE Trans. Biomed. Circuits Syst.*, vol. 9, no. 1, pp. 105–112, Feb 2015.

[6] P. A. Sundaram, D. L. Jean, E. M. Sparks, and M. A. Deeds, "Mechanical response of silicon mems diaphragms to applied pressure," *J. Microelectromech. Syst.*, vol. 23, no. 2, pp. 356–363, April 2014.

[7] W. Hemmert, M. Mermelstein, and D. Freeman, "Nanometer resolution of three-dimensional motions using video interference microscopy," in *12th IEEE Int. Conf. MEMS*, Orlando, FL, USA, Jan 1999, pp. 302–308.

[8] C. Gorecki, L. Salbut, and M. Jozwik, "Multifunctional interferometric platform for on-chip testing the micromechanical properties of mems/moems," *J. Micro/Nanolithography, MEMS, and MOEMS*, vol. 4, no. 4, pp. 041 402–1 – 041 402–5, 2005.

[9] W. Osten, *Optical inspection of microsystems*. CRC, Taylor & Francis, 2007.

[10] E. Novak, F. Pasop, and T. Browne, "Production metrology for mems characterization," in *2003 Symp. Design, Test, Integration and Packaging of MEMS/MOEMS*, 2003, pp. 295 – 299.

[11] J. Esteves, G. De Pasquale, L. Rufer, A. Koumela, S. Basrour, and A. Soma, "Experimental validation of diaphragms for acoustic microtransducers," in *Symp. Design, Test, Integration and Packaging of MEMS/MOEMS*, April 2015, pp. 1–4.

[12] A. Klein, A. Schroth, G. Gerlach, and R. Maeda, "Transient measurement of surface deflection for beams and membranes in micromechanical devices," in *Proc. SPIE*, vol. 3411, 1998, pp. 618–623.

[13] K. Gastinger, K. H. Haugholt, M. Kujawinska, M. Jozwik, C. Schaeffel, and S. Beer, "Optical, mechanical, and electro-optical design of an interferometric test station for massive parallel inspection of mems and moems," in *Proc. SPIE*, vol. 7389, 2009, pp. 73 891J–73 891J–12.

[14] Kujawinska and Gastinger, "An interferometric test station for massive parallel inspection of mems and moems," *Photonic Letter Of Poland*, vol. 1, no. 2, pp. 58–60, 2009.

[15] F. Oesterle, G. Vinci, and A. Koelpin, "A novel, w-band microwave based contactless test method for mechanical sensitivity analysis of mems," in *IEEEMTT-S Int. Microw. Symp. Dig*, Seattle, USA, Jul. 2013, pp. 1–4.

[16] F. Oesterle, M. Gardill, R. Weigel, and A. Koelpin, "Evaluation of a microwave based contact-free testing method for mechanical sensitivity analysis of mems for inline integration of on-wafer measurements," in *Eur. Microw. Conf.*, Nuremberg, Germany, Oct. 2013, pp. 72–75.

[17] S. Linz, F. Oesterle, A. Talai, S. Lindner, S. Mann, F. Barbon, R. Weigel, and A. Koelpin, "100 GHz reflectometer for sensitivity analysis of MEMS sensors comprising an intermediate frequency six-port receiver," in *2015 IEEE Conf. Wireless Sensors and Sensor Networks*, San Diego, USA, Jan. 2015, pp. 20–22.

[18] F. Oesterle, F. Fink, A. Dehe, H. Kuhn, R. Weigel, and A. Koelpin, "A large deflection model of silicon membranes for testing intrinsic stress of mems microphones by measuring pull-in voltage," in *Proc. SPIE Microtechnologies, Smart Sensors, Actuators, MEMS VI, Conference 8763*, Grenoble, France, Apr. 2013, pp. 1–11.

[19] S. Chowdhury, M. Ahmadi, and W. Miller, "Pull-in voltage study of electrostatically actuated fixed-fixed beams using a vlsi on-chip interconnect capacitance model," *J. Microelectromech. Syst.*, vol. 15, no. 3, pp. 639–651, June 2006.

[20] F. Serra Alves, R. Alves Dias, J. Cabral, J. Gaspar, and L. Rocha, "High-resolution mems inclinometer based on pull-in voltage," *J. Microelectromech. Syst.*, vol. 24, no. 4, pp. 931–939, Aug 2015.

[21] F. Oesterle, R. Weigel, and A. Koelpin, "A new approach on mems sensor batch testing using an analogue parallel test methodology for massive reduction of test time," in *Proc. IEEE Sensors*, Baltimore, USA, Nov. 2013, pp. 1–4.

[22] L. Rocha, E. Cretu, and R. Wolffenbuttel, "Analysis and analytical modeling of static pull-in with application to mems-based voltage reference and process monitoring," *J. Microelectromech. Syst.*, vol. 13, no. 2, pp. 342–354, April 2004.

[23] M. Sheplak and J. Dugundji, "Large deflections of clamped circular plates under initial tension and transitions to membrane behavior," *J. Appl. Mech*, vol. 65, no. 1, pp. 107–115, 1998.

[24] M. Rahman and S. Chowdhury, "A highly accurate method to calculate capacitance of mems sensors with circular membranes," in *IEEE Int. Conf. Electro/Information Technology*, 2009, pp. 178–181.

[25] M. Hiebel, *Fundamentals of Vector Network Analysis*, 2nd ed. Rohde & Schwarz, 2007.

[26] A. Singh, X. Gao, E. Yavari, M. Zakrzewski, X. H. Cao, V. Lubecke, and O. Boric-Lubecke, "Data-based quadrature imbalance compensation for a cw doppler radar system," *IEEE Trans. Microw. Theory Techn.*, vol. 61, no. 4, pp. 1718–1724, April 2013.

[27] M. Zakrzewski, A. Singh, E. Yavari, X. Gao, O. Boric-Lubecke, J. Vanhala, and K. Palovuori, "Quadrature imbalance compensation with ellipse-fitting methods for microwave radar physiological sensing," *IEEE Trans. Microw. Theory Techn.*, vol. 62, no. 6, pp. 1400–1408, June 2014.

Sarah Linz received the B.Sc. and M.Sc. degree in Electrical, Electronics and Communication Engineering from the Friedrich-Alexander University of Erlangen-Nuremberg, Germany, in 2010 and 2012, respectively. In 2013, she joined the Institute for Electronics Engineering, Friedrich-Alexander University of Erlangen-Nuremberg, as a Research Assistant. Her research interests include RF and millimeter-wave circuits for high- precision displacement sensors and six-port technology.

Florian Oesterle Florian Oesterle received the diploma in mechatronic engineering from Ulm University of Applied Sciences in 2010 and the Ph.D. degree in electronic engineering from the Friedrich-Alexander University of Erlangen-Nuremberg in 2014. He is currently working in the area of passive safety and driver assistance systems at Robert Bosch GmbH in Stuttgart.

Stefan Lindner was born in Kulmbach, Germany, in 1985. He received his diploma in Mechatronics in 2011 at the Friedrich-Alexander University of Erlangen-Nuremberg, Germany. Since 2012 he is with the Institute for Electronics Engineering, Friedrich-Alexander University of Erlangen-Nuremberg, Germany, conducting his PhD studies on research topics related to innovative radar technology based on the six-port receiver. Primarily he is working with system simulation, baseband design as well as digital signal processing.

Sebastian Mann was born in Nuremberg (Germany) in 1987. He received his diploma in Electrical Engineering in 2012 at the Friedrich-Alexander University of Erlangen-Nuremberg, Germany. Currently he is working as a research assistant at the Institute for Electronics Engineering, Friedrich-Alexander University of Erlangen-Nuremberg. His research interests are in the area of microwave circuits and components design. At present, he investigates on high precision 61 GHz radar sensors for industrial applications. Meanwhile he's also working on different industrial projects based on the six-port interferometer technique.

Robert Weigel was born in Ebermannstadt, Germany, in 1956. He received the Dr.-Ing. and Dr.-Ing.habil. degrees in electrical engineering and computer science from the Munich University of Technology, Munich, Germany, in 1989 and 1992, respectively. From 1982 to 1988, he was a Research Engineer, from 1988 to 1994, a Senior Research Engineer, and from 1994 to 1996, a Professor of RF circuits and systems with the Munich University of Technology. In winter 1994/1995, he was a Guest Professor of SAW technology with the Vienna University of Technology, Vienna, Austria. From 1996 to 2002, he has been Director of the Institute for Communications and Information Engineering at the University of Linz, Austria. In 2000, he has been appointed a Professor for RF Engineering at the Tongji University in Shanghai, China. Since 2002 he is head of the Institute for Electronics Engineering at the Friedrich-Alexander University of Erlangen-Nuremberg, Germany.

Alexander Koelpin received his diploma in Electrical Engineering in 2005, his doctoral degree in 2010, and his venia legendi in 2015 at the Friedrich-Alexander University of Erlangen-Nuremberg, Germany. Since 2005 he is with the Institute for Electronics Engineering, Friedrich-Alexander University of Erlangen- Nuremberg, Germany, and since 2007 team leader Circuits, Systems and Hardware Test. His research interests are in the areas of microwave circuits and systems, wireless communication systems, local positioning, and six-port technology.